SIMULATION OF SEMICONDUCTOR DEVICES AND PROCESSES Vol. 4
Edited by W. Fichtner, D. Aemmer - Zurich (Switzerland) September 12-14, 1991 - Hartung-Gorre

Simulating Temperature Effects in Multi-dimensional Silicon Devices with Generalized Boundary Conditions

Kevin Kells Stephan Müller Wolfgang Fichtner
Integrated Systems Laboratory, ETH-Zentrum, 8092 Zurich, Switzerland

Gerhard Wachutka
Quantum Electronics Laboratory, ETH-Hönggerberg, 8093 Zurich, Switzerland

Abstract

We have developed a device simulator which, apart from solving the Poisson, electron, and hole equations, is capable of analyzing heat generation and conduction in 1, 2, and 3-dimensional silicon devices. A mechanism to allow generalized temperature boundary conditions, including inhomogeneous Neumann and mixed boundary conditions, has been implemented. We have applied this simulator to a 2-D MOS-controlled thyristor and a 3-D temperature sensor.

The ability to simulate the heat generation and temperature distribution within semiconductor devices is becoming increasingly important to allow the accurate simulation of a device's electronic, optical, and sensing properties. Non-isothermal conditions play an important role in device performance, for example, in semiconductor lasers, power devices, and microsensors. Even in the fields of VLSI and ULSI, accurate simulation of self-heating effects is becoming more important as integration densities and thereby power density dissipation continue to increase.

We have implemented the rigorous thermodynamic treatment of temperature and heating effects presented by Wachutka [1]. Here, the well-known current continuity equations for electrons and holes are extended to include a new driving force proportional to the gradient of the temperature T:

$$\vec{J}_n = -q\mu_n n(\nabla\phi_n + P_n\nabla T) \tag{1}$$

$$\vec{J}_p = -q\mu_p p(\nabla\phi_p + P_p\nabla T). \tag{2}$$

q is the electronic charge, n and p are the densities, ϕ_n and ϕ_p are the quasi-fermi levels, μ_n and μ_p are the mobilities, and P_n and P_p are the thermoelectric powers[1] for the electrons and holes, respectively. The electron and hole gases are assumed to be in thermal equilibrium with the lattice, hence, $T = T_{\text{latt}} = T_{\text{e}} = T_{\text{h}}$.

In additional to solving the three electronic equations, we introduce a fourth equation relating the temperature T with the heat generation rate H:

$$-\nabla\cdot\kappa\nabla T = H, \tag{3}$$

where κ is the thermal conductivity. The heat generation rate H is defined as the sum of the Joule heats due to electron and hole current, H_{J_n} and H_{J_p}, the recombination heat H_{rg}, and

[1] We follow the experimental notation where $P_n < 0$, whereas Wachutka assumes $P_n = |P_n|$. This is reflected in the sign reversal in our electron equation with respect to Wachutka's formula.

the Thomson heat H_{Th}. These quantities are defined as follows in the steady-state:

$$H_{J_n} = \frac{|\vec{J}_n|^2}{q\mu_n n}, \qquad H_{J_p} = \frac{|\vec{J}_p|^2}{q\mu_p p}, \tag{4}$$

$$H_{rg} = qR\Big[\phi_p - \phi_n + T(P_p - P_n)\Big], \tag{5}$$

$$H_{Th} = -T\Big(\vec{J}_n \cdot \nabla P_n + \vec{J}_p \cdot \nabla P_p\Big), \tag{6}$$

where $\vec{J}_n$ and $\vec{J}_p$ are the electron and hole charge current densities and R is the recombination rate. Equation (6), the Thomson heat, is neglected.

1 Discretization

We solve the point-divergence form of the extended current continuity equations, introducing an integration factor with varying T. [2] The resulting discretized electron current continuity equation is defined in terms of the Bernoulli function $\mathcal{B}$ (using the scaling scheme of de Mari [3]):

$$J_n = \frac{\mu_n}{\Delta x} T_{i+1/2}\Big[n_{i+1}\mathcal{B}(-\beta_n) - n_i\mathcal{B}(\beta_n)\Big] \tag{7}$$

where

$$\beta_n = -\Big[\Delta\psi + T\Delta\ln n_{ie} + \Big(\ln\frac{n_{ie}}{n} + P_n\Big)\Delta T\Big]\Big(T_{i+1/2}\Big)^{-1} \tag{8}$$

Here, ψ is the electrostatic potential, n_{ie} is the effective intrinsic density, Δx is the distance between point i and point $i+1$, and the subscript $i+1/2$ represents an average of the values at x_{i+1} and x_i. The thermoelectric powers P_n and P_p are computed using bicubic splines fitted to data presented by T. Geballe and G. Hull [4]. By letting $\Delta T = 0$, the Scharfetter-Gummel expressions for both electrons and holes are recovered.

2 Boundary Conditions

We have the capability of handling general boundary conditions, including inhomogeneous Neumann and mixed conditions. Using the box discretization, we end up with the following form for the temperature equation:

$$\sum_{i \neq j} \kappa_i \left(\frac{\partial T}{\partial N}\right)_{ij} d_{ij} + H_i V(\Omega_i) = 0 \tag{9}$$

where H_i is the heat generation rate inside the integration box Ω_i and $V(\Omega_i)$ is the volume of the box. For non-interface points, we discretize the normal derivative of the temperature:

$$\left(\frac{\partial T}{\partial N}\right)_{ij} = (T_j - T_i)\frac{1}{l_{ij}} \tag{10}$$

where l_{ij} is the distance between grid points i and j.

At the interface with thermal contacts, we are free to choose an arbitrary function for the normal derivative of the temperature, $\partial T/\partial N$. At non-ideal thermal contacts, we implement

Newton's law of cooling, also known as the *radiation* boundary condition [5]. We introduce "twin" points i and i' for each node i at thermal contacts (see Figure 1). Using linear heat transfer theory at the interface, the normal derivative of the temperature reads:

$$\kappa_i \left(\frac{\partial T}{\partial N} \right)_{ii'} = h_{ii'} (T_{i'} - T_i), \tag{11}$$

where $h_{ii'}$ is the *surface heat conductance* or the *coefficient of surface heat transfer*. This value is chosen by the user to characterize the quality of the thermal contact.

3 Examples

3.1 Thermopile

We simulated a silicon thermopile (see, for example [6]) in three dimensions. The operation of this device is based on the Seebeck effect, where a potential is built up in a semiconductor due to a temperature gradient across the device. A number of p-doped silicon wells are connected in series to enhance this effect.

A temperature difference ranging from 0.05 K to 18.0 K was applied to the ends of the device using Dirichlet boundary conditions. The resulting linear behavior of the hole quasi-fermi-level, as well as the temperature distribution and the hole quasi-fermi-level distribution for a temperature difference of 10 K are shown below.

3.2 MCT

Our second example consists of a 2-dimensional MOS Controlled Thyristor (MCT) simulated in the latched state, including temperature effects. Here, we use radiation boundary conditions to simulate realistically the imperfect cooling of the device through the contacts. As a comparison, we show the temperature distribution inside the MCT when simulated with ideal thermal boundary conditions. The surface heat conductance for the radiation boundary conditions was chosen to be 15 $W/K\,cm^2$.

References

[1] G. K. Wachutka, "Rigorous thermodynamic treatment of heat generation and conduction in semiconductor device modeling," *IEEE Trans.*, vol. CAD-9, pp. 1141–1149, 1990.

[2] T.-W. Tang, "Extension of the Scharfetter-Gummel algorithm to the energy balance equation," *IEEE Trans. on Elec. Dev.*, vol. ED-31, pp. 1912–1914, 1984.

[3] A. de Mari, "An accurate numerical steady-state one-dimensional solution of the p-n junction," *Solid-State Electron.*, vol. 11, pp. 33–58, 1968.

[4] T. H. Geballe and G. W. Hull, "Seebeck effect in silicon," *Physical Review*, vol. 98, pp. 941–947, May 1955.

[5] H. S. Carslaw and J. C. Jaeger, *Conduction of Heat in Solids.* Oxford, England: Oxford University Press, 1978.

[6] S. Middelhoek and S. A. Audet, *Silicon Sensors.* London, England: Academic Press Limited, 1989.

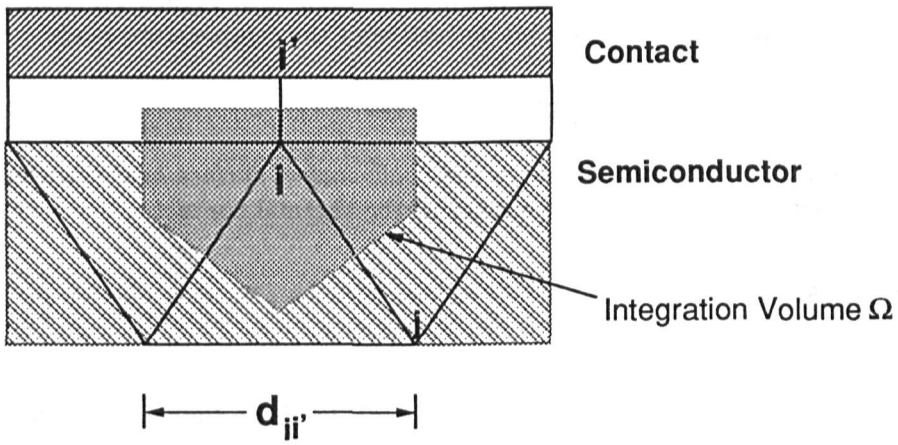

Figure 1: Boundary conditions at a thermal contact

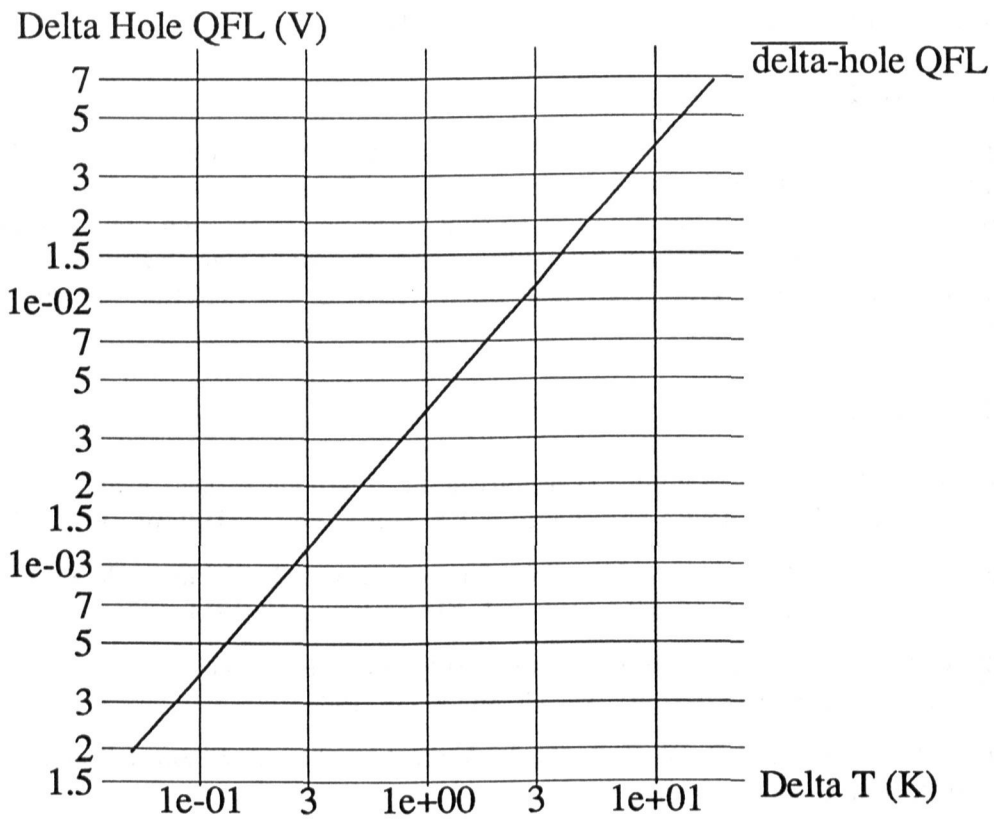

Figure 2: Difference of the hole quasi fermi level at both contacts as a function of temperature (log scale).

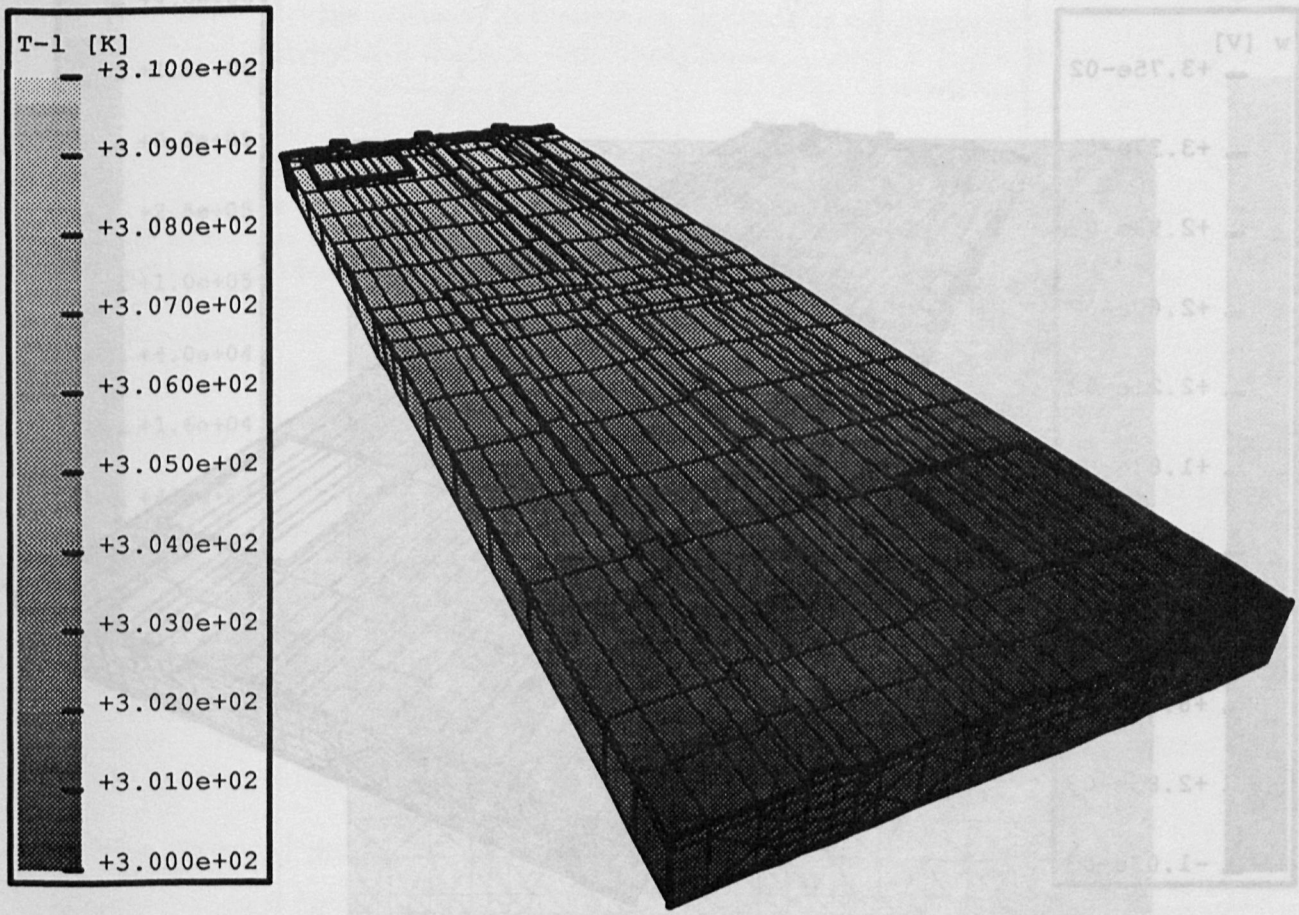

Figure 3: Temperature distribution in the sensor device.

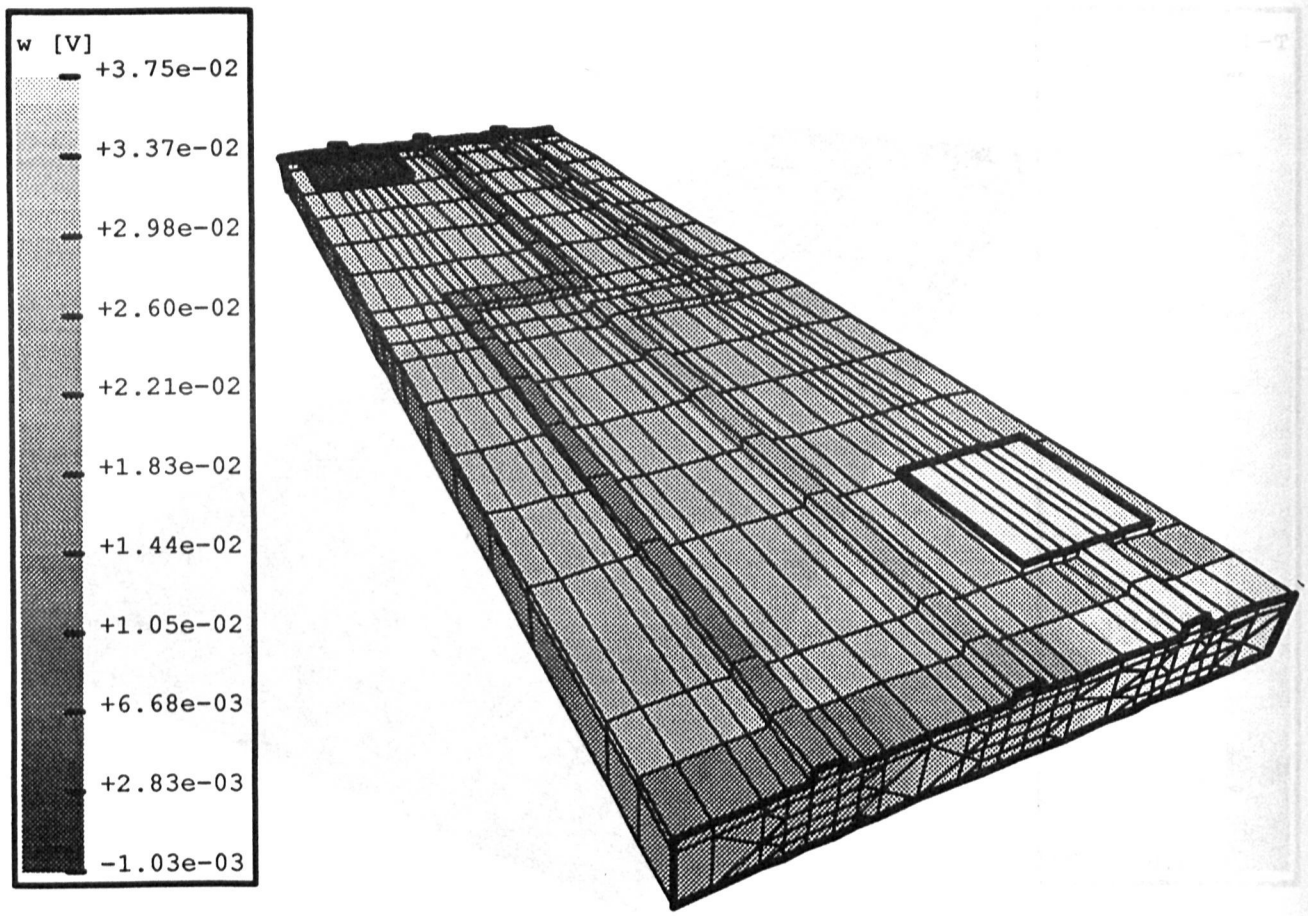

Figure 4: Hole quasi-fermi-level in the sensor device.

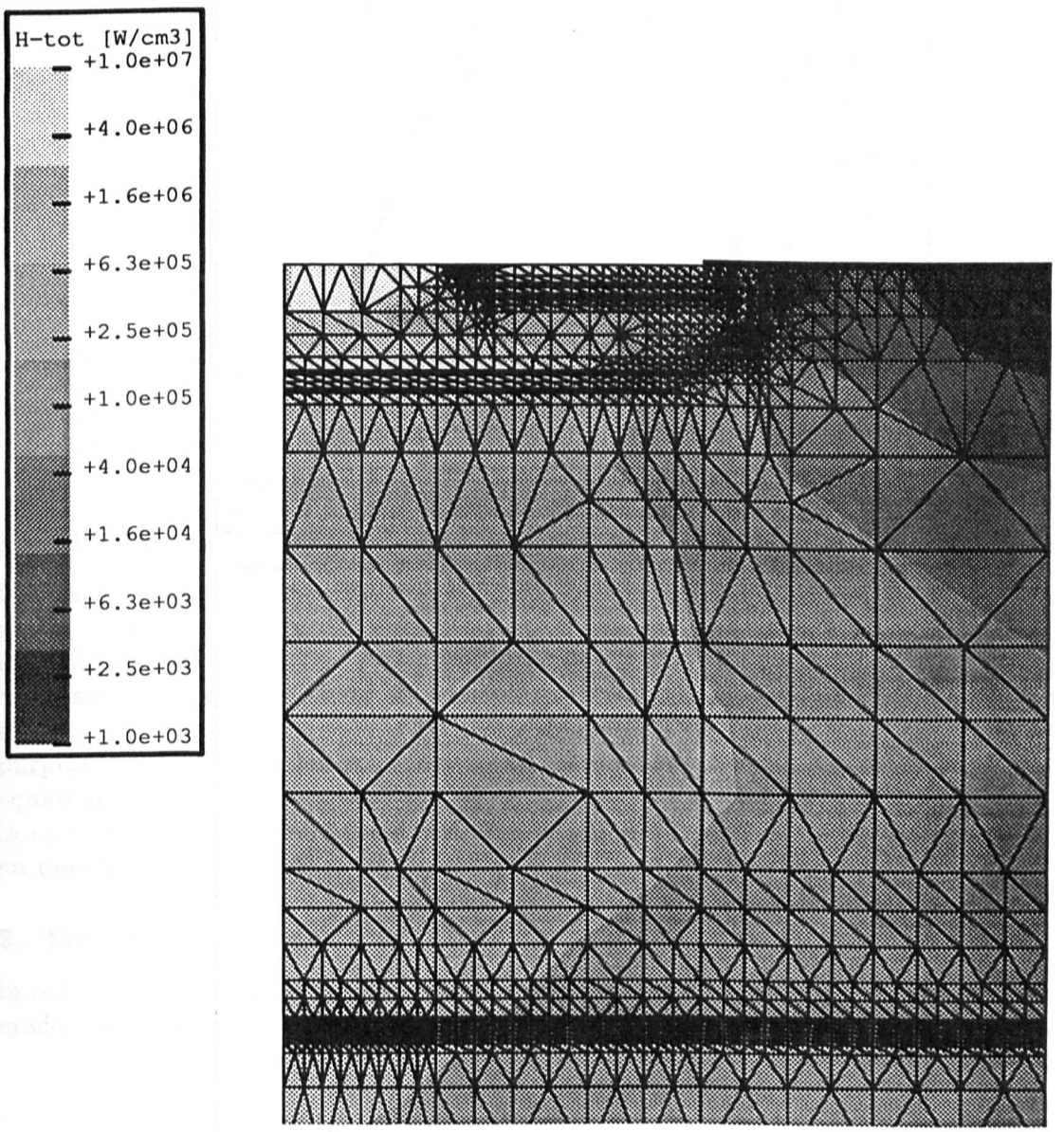

Figure 5: Total heat generation of close-up of MCT, simulated with radiation boundary conditions

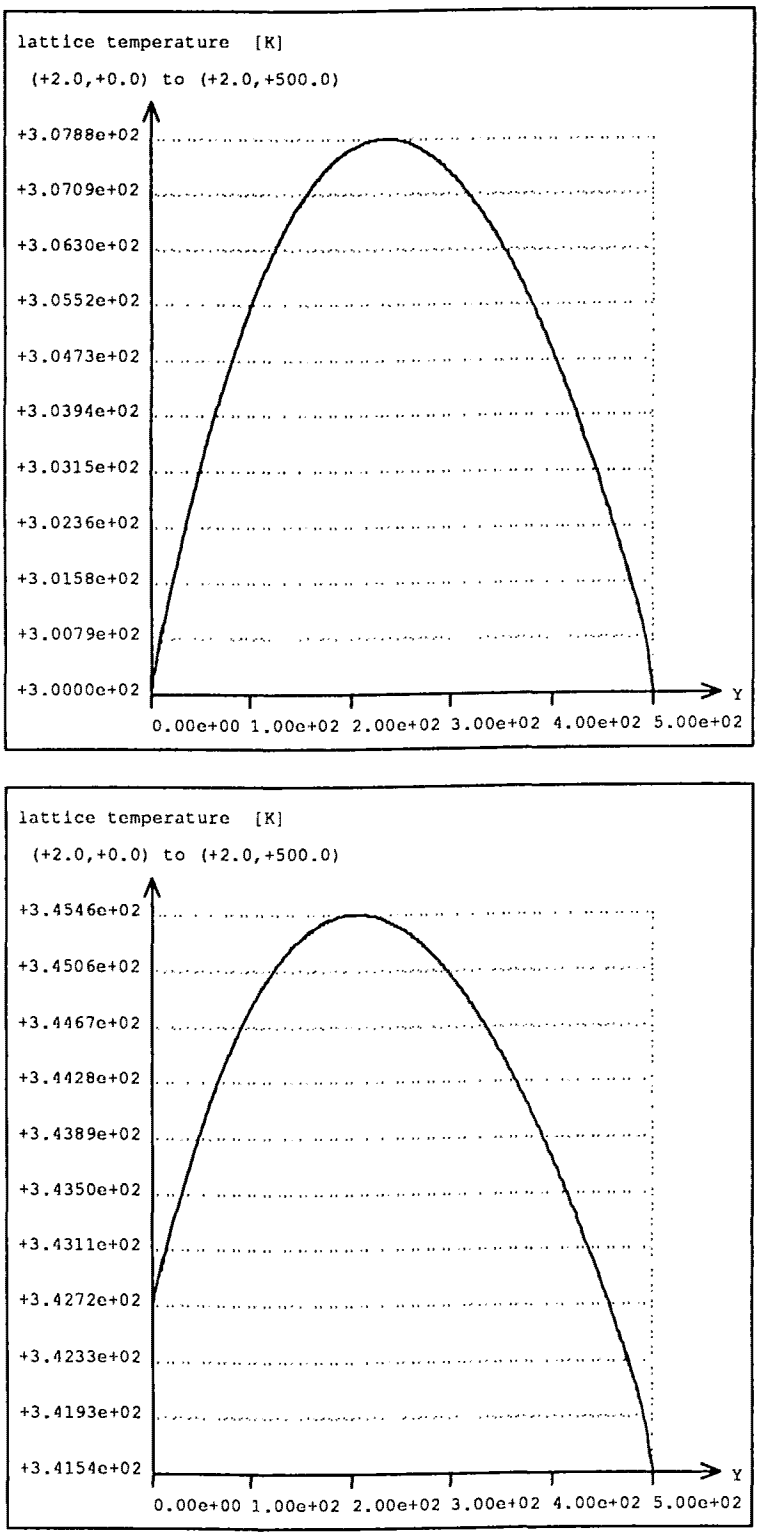

Figure 6: Temperature distribution in the MCT measured inside the device from cathode ($x = 0$) to anode ($x = 500$) with Dirichlet (top) and radiation boundary conditions. (Note differing scales)